International Refereed Journal of Engineering and Science (IRJES)
ISSN (Online) 2319-183X, (Print) 2319-1821
Volume 7, Issue 8 Ver. I (Aug 2018), PP. 01-11

Atomic Layer Deposition of TiO_2 From Tetrakis (Dimethylamino) Titanium And H_2O On Commercial-Grade Iron: A Simple Method For Support Preparation

Jose Domingo Gonzalez-Ramirez*, Maricela Villicañamendez*, Hugo Tiznado-Vazquez**, Gabriel Alonso-Nuñez**, Jose Apolinar Cortes*

** (División de Estudios de Posgrado de la Facultad de Ingeniería Química, Universidad Michoacana de San Nicolás de Hidalgo, Avenida Francisco J. Múgica S/N, Ciudad Universitaria, 58030, Morelia, Michoacán, México)*

*** (Centro de Nanociencias y Nanotecnología, Universidad Nacional Autónoma de México, km 107 Carretera Tijuana-Ensenada, P.O. Box 14, 22800, Ensenada, Baja California, México)*

Corresponding Author:Jose Apolinar Cortes.

ABSTRACT:*This report describes a titanium dioxide (TiO_2) atomic layer deposition (ALD) on a commercial-grade iron substrate from tetrakis (dimethylamino) titanium (TDMAT) and de-ionized water as titanium and oxygen precursors, respectively. This particular substrate was prepared in a short period of time (approximately 20 min) by a simple procedure, which could represent a new and interesting option to elaborate thin films through an ALD process. The TiO_2 deposition was studied at the support temperature of 225°C. The number of ALD cycles was varied in the range of 50 cycles to 250 cycles, and the effects of this parameter were investigated. Samples were characterized by XPS, XRD, RS, SEM and AFM analyses in order to scrutinize their composition and microstructure. TiO_2 films grew as anatase phase, which was gradually developed with a rising number of ALD cycles. XPS indicated a moderate silicon contamination due to sandpapers used during the substrate preparation, which was similar for all samples. However, the morphology and topography of these layers were clearly determined by the iron support surface. Rough TiO_2 films were obtained with RMS roughness of at least 89 nm.*

KEYWORDS*: TiO_2; TDMAT; Atomic layer deposition; Iron support; Wustite; Raman spectroscopy.*

Date of Submission:22-11-2018 Date of acceptance: 07-12-2018

I. INTRODUCTION

Titanium dioxide (TiO_2) is a semiconductor that has unique features [1][2][3] favoring versatile uses [4][5][6], although the most important application currently is in the photocatalysis systems [7], since anatase TiO_2 is indeed recognized as the most efficient photocatalytic material [8]. Intensive efforts are still being devoted to this semiconductor's fabrication [9].

Many of the applications of TiO2 are performed with thin layers on either planar or three-dimensional supports [10], and atomic layer deposition (ALD) facilitates its growth onto numerous supports such as these with an accurate control of thickness. ALD allows a homogeneous deposition with conformality, precise control of composition and good reproducibility [11]. Additionally, the ALD films do not need further post-annealing treatment to be crystallized, since substrates are in-situ heated [12], and they are firmly bound to the substrate [13]. All of these characteristics are the reason why the ALD route has attracted attention for TiO_2 thin film deposition [14].

ALD is a gas-phase coating method based on two saturation half-reactions, where the layer precursors are separated during their deposition. The precursor pulses are commonly separated by a nitrogen purge. After the precursors have reacted, the surface is reactivated for another similar cycle; the cycles are repeated until the desired thickness has been achieved [15].

Titanium alkoxides and halides are typically used as titanium precursors coupled with H_2O as an oxidant for ALD-TiO_2 [16]. Tetrakis (dimethylamino) titanium (TDMAT) has been proposed in recent years as a good option for titanium precursor, since its decomposition products are non-toxic and non-corrosive [17]. TDMAT thermal gas phase decomposition is observed at 300°C or higher temperatures [10].

However, substrates utilized for ALD-TiO_2 are simply purchased with valid features to be used as delivered; otherwise, they are usually prepared by robust treatments. Monocrystalline (100) oriented silicon materials have been comprehensively utilized for it as substrates; they can undergo etching procedures [18][19][20]. Mirror-polished surface for metal supports is attained after a long polishing process in addition

[15]. With these treatments in mind, a simplistic and brief method of preparation for an adequate ALD-TiO_2 substrate is desirable.

In this respect, this work focuses on the assessment of TDMAT and H_2O as sources of titanium and oxygen, respectively, for ALD-TiO_2 onto a commercial-grade iron support. The support is potentially suitable for the deposition of TiO2, since it is certainly affordable and highly available, but it will be also interesting due to its simple and feasible preparation procedure compared to publications cited above. The influence of these specific parameters on the elaborated samples will be determined by a systematic investigation of the physicochemical properties. TiO_2 deposition on this iron substrate represents the first step toward a detailed exploration in various research fields, e.g., photocatalysis or analogous processes, owing to its ability to overcome the main drawbacks of TiO_2 particle slurries [21][22]. However, these studies may have more significance in the search for new substrates for ALD-TiO2 with the aforementioned features of our particular substrate.

II. EXPERIMENTAL DETAILS

2.1Atomic layer deposition

TiO_2 films were grown in a custom-built flow-type ALD reactor from TDMAT (99.999%, Sigma-Aldrich) and de-ionized H_2O as titanium and oxygen precursors, respectively. TDMAT was heated in a metal reservoir and thermostated to 60°C before the ALD process, whereas a lateral reservoir contained the de-ionized H_2O at room temperature. Nitrogen was used as purging gas for precursors and their gaseous by-products at a working pressure of ~20 mTorr, which was purified and supplied by an inert gas purifier Centorr/Vacuum, model 2A.

A commercial-grade raw iron piece measuring approximately 1 mm in thickness was mechanically cut into smaller square pieces of 1.5 cm × 1.5 cm in order to finally employ them as supports for the TiO_2 deposition. By initiating a preparation of these materials for the ALD reactions, an oily coverage was wiped off by a cotton cloth from their surfaces. After that step, a manual polishing was gently performed on them by two different silicon carbide sandpapers (firstly 180 grit and then 1000 grit); ethanol was used to rinse the metal surface during polishing. Ultimately, the metal pieces were ultrasonically cleaned during 5 min with acetone, and next, they were immediately blown free of acetone with pressurized air before loading them into the ALD reactor chamber. This type of preparation for every substrate took an estimated time of 20 min.

A substrate was laid on the reactor sample holder and heated to reach a substrate temperature (TS) set at 225°C prior to the ALD process. Iron substrates were kept in the reactor chamber for 10 min at TS in order to accomplish a thermal equilibrium through the entire material, while a simultaneous purge was performed (throughout heating). ALD reactions began after that step with several numbers of ALD cycles for each support.

The number of ALD cycles significantly varied between 50 cycles and 250 cycles with increments of 50 cycles, although the TDMAT or de-ionized H_2O exposure times and their programmed purge duration were constant for all of our experiments. An ALD cycle comprises 0.15 s of TDMAT pulse, 30 s of purge, 0.10 s of de-ionized H_2O pulse, 20 s of purge and 20 s to reach the working pressure, which is required by the chamber for the next cycle. The elaborated samples are designated 50-C, 100-C, 150-C, 200-C, and 250-C, the numbers of which indicate the selected number of deposition cycles for their fabrication; the 0-C sample refers to the bare iron support.

2.2Characterization

Surface compositions from our specimens were identified by X-ray photoelectron spectroscopy (XPS). These fine determinations were measured by a high-resolution X-ray photoelectron spectrometer SPECS FlexMod system equipped with a monochromatized Al Kα X-ray source (1486.6eV). The XPS peak positions were calibrated by using the C-C bond signal from the adventitious hydrocarbon contamination with a C 1s binding energy of 284.5 eV. Data were collected through a concentric hemispherical energy analyzer with multichannel detection at an operating power of 25 W. Surface concentrations of titanium and oxygen were estimated from XPS spectra with the OriginPro 9.0.0 software package by using their peak area. Chemical states were also investigated for the primary constituents.

Microstructural investigations were conducted by X-ray diffraction (XRD) to scrutinize the film and substrate crystalline phases and their crystallinity. Conventional XRD measurements were performed at room temperature by a Philips X'Pert MPD diffractometer with Cu $K\alpha_1$ (λ=0.154056 nm) radiation at an accelerating voltage of 45 kV and an emission current of 40 mA. Diffraction patterns were acquired in a step of 0.04°/s for 2θ angular ranges from 20° to 90°. Raman spectroscopy (RS) provided complementary microstructural studies. The Raman spectra were recorded at room temperature with an HORIBA XploRA Raman spectrometer equipped with an optical microscope. The spectral resolution was 4 cm^{-1} over the range from 100 cm^{-1} to 1000 cm^{-1}, and the power of the incident laser beam on the samples was approximately 10 mW with an excitation wavelength of 514 nm. A silicon reference sample was used for the calibration of the Raman shift.

Atomic force microscopy (AFM) was performed by a Park Systems XE-70 microscopy system for the surface topography characterization. Samples were examined in air with a standard silicon cantilever in contact mode at a scanning frequency of 0.7 Hz. Distinct square maps of 7.5 μm from different sites of any sample were performed in order to check its root-mean-square (RMS) surface roughness; the XEI v.1.8.0 software package was used to obtain this parameter, where no image processing, except flattening, was applied on the maps. Additional information for the surface morphology was analyzed with a scanning electron microscope and a focused ion beam (SEM-FIB) JEOL JIB-4500 MultiBeam system at an accelerating voltage of 15 kV.

III. RESULTS AND DISCUSSION

3.1Preliminary assessment

The TiO_2 depositions were tested without experimental disturbances, and a slight non-homogenous color change on the surface of samples was visually detected; the more ALD cycles there are, the darker the color on the sample surface is. This effect could be opportunely attributed to a growing thickness of the TiO_2 layer, since it is an argument congruent with ALD cycles; however, a phenomenon similar to this is demonstrated in our previous experiments for the bare support at a similar temperature and analogous times of heating. It is worth mentioning that this color changing for the elaborated samples is less intense than that for the other specimens, which suggest that TiO_2 layers hinder this surface alteration.

3.2Film properties

3.2.1Composition

The XPS technique is highly sensitive to any material surface [20][23]; therefore, it paved the way to elucidate compositions and chemical states of the main constituents, such as Ti and Fe, from our samples. This tool was, in turn, decisive for verifying whether the TiO_2 deposition is achieved.

Fig. 1 depicts XPS spectra with respect to samples 0-C, 50-C, 150-C, and 250-C. Several peaks for O, Ti, Fe and even Si signals are seen in the abscissa range of 0 eV to 200 eV. The intensities for Fe peaks are gradually debased until they disappear insofar as the number of ALD cycles rises; their intensities may become weak in order to demonstrate that the support surface is being covered, since iron is the main element in our supports, which consequently means that a TiO_2 deposition is virtually fulfilled. Conversely, Ti signals follow a completely opposite behavior to those of Fe, which ensures an increasing Ti deposition that it is initiating at 50 ALD cycles. O peaks keep the same tendency as those of Fe peaks, and it could imply that both elements are related, that is to say, they are part of the bare support. Si signals are prone to appear due to the silicon carbide sandpapers employed during the polishing procedure, since they are the only feasible source to introduce silicon impurities onto the bare-support surface, although their intensities follow an ambiguous behavior that can be attributed to random silicon contents in the supports; because of the 0-C sample spectrum with no Si peaks, these impurities should be retained either close to the film surface or underneath it. Silicon impurities could be embedded in either surface dents or scratches, which are studied in the upcoming section 3.2.2.

The C 1s signal indicates the existence of residual carbon in spectra, and this is checked for all of these samples, although it is difficult to distinguish any peak among those signals because they almost overlapped. Their intensity nevertheless maintains no apparent trends as before, but we observe an order like 50-C>0-C>150-C=250-C that presumably involves an inevitable surface carbon contamination. Aariket al.[20] reported that carbon contamination is frequently induced by some kind of titanium precursors (TDMAT included) when they are deposited at 225°C or lower temperatures, and it is, therefore, something to expect under our working conditions. Since carbon intensities are not in agreement with a rising number of ALD cycles, carbon introduction must be strongly governed by the naturally-adsorbed atmospheric carbon contributions [19][20] to explain the lack of a trend in this case.

Nitrogen residues originated by an incomplete dissociation for the titanium precursor molecule were investigated on the surface of these specimens, and it seems that this process alteration was blocked in our experiments, as they were not found at all. Comparable results were obtained by Xieet al.[18], but they mentioned that the Ti-N bond in TDMAT was fully broken (at least to the detection limit of XPS). Other researchers, such as Abendrothet al.[10], have obtained contradictory results with TDMAT, and they noticed a growing nitrogen concentration as T_S increased (maximum value of 6±2at.% at T_S=320°C); whereas Kanomataet al.[19] detected a nitrogen peak at room-temperature ALD process, thereby indicating that nitrogen in TDMAT was not thoroughly removed by their system (plasma-excited water vapor).

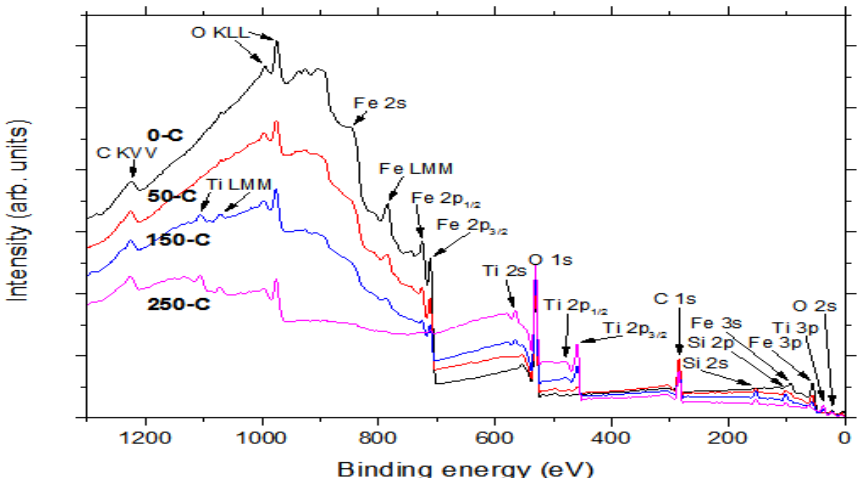

Fig. 1.XPS wide-scan spectrum for the fabricated samples 0-C, 50-C, 150-C and 250-C by the ALD method from TDMAT and H_2O at a substrate temperature of 225°C.Peaks indexation was taken from the XPS instrument database.

Upper binding energy values reveal Ti and Fe signals with the behavior that was already described, which is better seen in Fig. 2 and 3, respectively. The O 1s signal tendency is equal to that of Ti signals, while it is in opposition to O 2s signal behavior; as we rationalized before, this could advise that Ti and O 1s peaks are correlated as a single chemical compound (titanium oxide). Because of ALD cycles number variation, Ti and Fe peaks are constantly changing their maximum intensity position in the spectra. In general, those peaks change from a particular binding energy to higher binding energies in the same way as ALD cycles increase. As we will discuss for titanium peaks, these observations may suggest that elements are oxidized during the ALD process and their oxidation level could be indirectly determined by the ALD cycles. Preparation procedure for substrates could develop partially oxidized surfaces, where oxidation processes primarily take place.

An estimated Ti 2p:O 1s ratio of approximately 1:1.9 is obtained for our samples by analyzing the intensities for TiO_2 doublet peaks (Ti $2p_{1/2}$ and Ti $2p_{3/2}$), along with their corresponding O 1s intensity [18][19][20][24][25][26], which roughly represents the stoichiometric composition of TiO_2 formula that progressively grows on the support surface with an increasing number of ALD cycles [14][17][19]. Certain deviations of the Ti 2p peaks as those of Fe 2p peaks are noted during the inspection of photoelectron spectra in Fig. 2; hence, we can corroborate a rising oxidization state for Ti 2p in addition. For a similar observation, Kanomataet al.[19] argued that titanium in TiO_2 is not fully oxidized. Xieet al.[18] and Liu et al.[27] agree with them, thus mentioning that either an asymmetric Ti 2p spectra or a chemical shift might indicate an incomplete oxidation of titanium.

Small peaks located at binding energies of approximately 926 eV, 937 eV and 904 eV could not be assigned to any aforementioned element, although a careful identification was performed. However, these peaks should derive from support components rather than those of film, since they are more defined for the bare-support spectrum and they slowly decrease insofar as ALD cycles increase. Information about these peaks is not sufficient for their identification, but they could be also assigned to any auger transition for iron due to their binding energy.

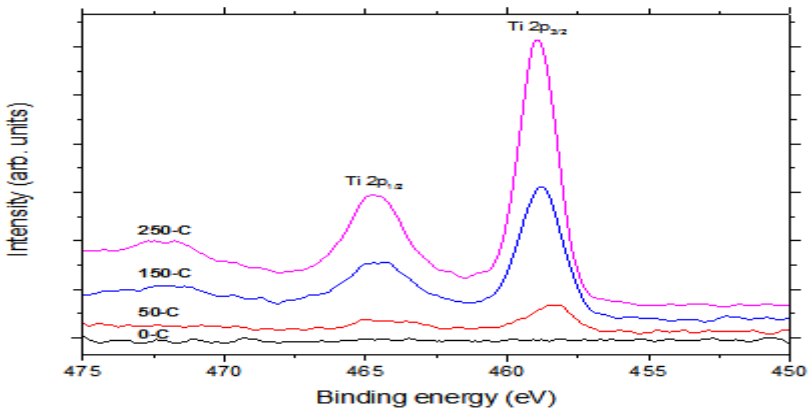

Fig. 2.Ti 2p spectra graphPeaks indexation was taken from the XPS instrument database.

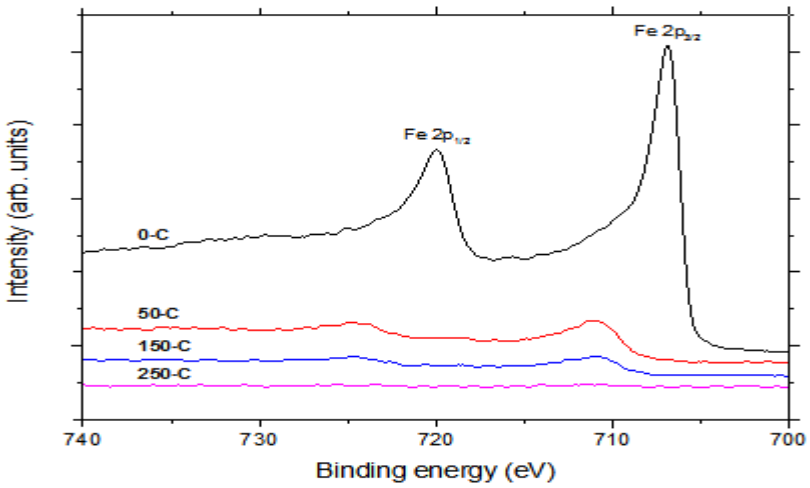

Fig. 3.Fe 2p spectra graph. Peaks indexation was taken from the XPS instrument database.

3.2.2Microstructure

Fig. 4 shows the XRD patterns regarding our samples and somehow, reflections related to crystalline TiO_2 are not obviously found in these diffractograms. This feature is attributed to a low content of TiO_2 (thin film) on the substrate surface and the detection/resolution limit of the diffractometer used in this study [25][26][28][29], as well as a probable poor crystallinity for the film. A faint TiO_2 presence is able to be identified by an equipment with a suitable detection limit, but even so, the equipment misses the TiO_2 signals if this material is not considerably crystallized in order to undergo a diffraction phenomenon and be detected in turn. The specimen 250-C was additionally examined by glancing angle X-ray diffraction (GAXRD) (data not shown here) in order to enhance its detection by suppressing most of the contributions from the substrate; the penetration depth of the X-rays is confined to the near surface area at small angles of incidence [10][20]. TiO_2 crystalline phases were not exposed by GAXRD, although in this sample, it should have grown the thickest and most crystallized film among the other ones due to its elaboration conditions. We consequently outline the TiO_2 XRD analyses as a matter of a thin film that cannot be detected, since it is under the detection limit.

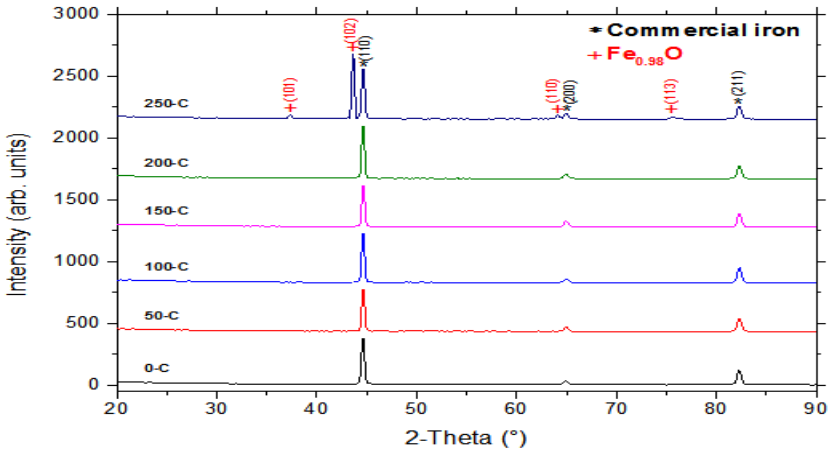

Fig. 4.XRD results for the samples elaborated by the ALD method from TDMAT and H_2O from 50 ALD cycles to 250 ALD cycles at a substrate temperature of 225°C. The reference positions of the commercial iron (asterisks) and $Fe_{0.98}O$ (crosses) reflections are marked as well.

Only Bragg reflections from the iron support are visible, and the diffraction angles of 44.67°, 65.02°, and 82.33° are ascribed to those of commercial/synthetic iron crystal planes (110), (200), and (211), respectively. All of these samples, except for 250-C, comprise a unique crystalline phase with a preferred (110) orientation. Peaks at 37.83°, 43.52°, 64.22°, and 75.51° that correspond to $Fe_{0.98}O$ crystal planes (101), (102), (110), and (113), respectively, in conjunction with those of commercial iron phase, coexist in 250-C as two polycrystalline phases. In this case, a dominant peak located at 43.52° is more prominent than that of commercial iron; hence, this new phase is displacing the other one, and it should be present in a significant proportion in the sample; further, it could improve its crystallinity in comparison with the original phase.

Crystalline phases were identified with PDF#06-0696 (syn. iron) and PDF#39-1088 ($Fe_{0.98}O$) from a powder diffraction file database, where reflections with minimum relative intensities were neglected, since they were not observed in these XRD patterns.

The spontaneous appearance of this particular iron oxide is not trivial, and the actual circumstances involved in its formation are uncertain at this moment due to this phenomenon not being expected, but they will be argued in the next paragraphs. However, the TiO_2 film must be responsible for this occurrence up to a certain degree owing to the aforementioned experiments for the bare support at a similar temperature and analogous times of heating, which did not show reflections for $Fe_{0.98}O$. A long exposure time (almost 5 h) at a temperature of 225°C, i.e., a thermal treatment, along with an incomplete oxidation for supports in accordance with our previous XPS results tentatively promoted the appearance of that iron oxide in addition to the fact of a TiO_2 deposition [26]; the thermal treatment could begin to oxidize the support surface and a TiO_2 layer can block this process in order to obtain this formation.

In agreement with the literature, the deposition temperature played an important role in the crystalline phase and its content [30]; furthermore, the development of a certain crystalline structure of deposited TiO_2 films depends on the precursor and a critical thickness in non-epitaxial films [20]. In most cases, the crystallographic anatase nevertheless takes place at ca. 200°C, while rutile form starts to crystallize at 350°C or 400°C without the necessity of a post-annealing treatment, and films mostly comprise an amorphous phase below 200°C [13][18]. Abendrothet al.[10] singularly elaborated a thin film with anatase and rutile termination for T_S above 250°C, but this film is explained by a CVD-type deposition, where the decomposition mechanism of TDMAT changes from dominated at the surface to surface plus gas phase decomposition at the same temperature range.

It is therefore noteworthy that anatase phase might be fulfilled for our samples under the selected T_S, although we cannot prove it with XRD investigations. This principle is promising for the catalytic activity since the anatasephotocatalyst is often considered to be the most reactive crystal structure of TiO_2 under UV light illumination because of its larger band gap than that of rutile [8][9][12][14][31][32]. However, the photocatalytic effect is drastically diminished with the amorphous phase due to its lattice defects, either in the bulk or on the surface of any film, which provide recombination centers for photogenerated electron-hole pairs, thereby reducing the charge carriers concentration that this effect needs [9][33]. Despite the TiO_2 structure, the efficiency of a photocatalytic material might be quite dependent on the type of pollutant to be removed [34].

It was difficult to search a small TiO_2 portion on the support through the XRD technique; therefore, the RS method was used to explore the TiO_2 crystalline information. Raman scattering measurements were still tackled on the same samples as those for the XRD study in order to verify their structural changes. Supplemental information upon the overall amount of anatase was, moreover, expected since this method is less sensitive to the orientation of crystallites than XRD [20], and it is more sensitive to the Raman signature of anatase and amorphous phases than that technique [14].

Fig. 5 belongs to our Raman spectra, where three main Raman-active peaks located at 305 cm^{-1}, 521 cm^{-1}, and 648 cm^{-1} are clearly seen for 250-C. It is easy to note that the most intense peak at 648 cm^{-1} emerged as ALD cycles increased, and the other ones were rarely seen up to 200-C. Minor peaks are either blurred or imperceptible for the other samples. This phenomenon is similar to the appearance of $Fe_{0.98}O$ in the XRD studies since it is only observed in 250-C diffractogram, and we may think that both their results are related; thus, they can complement each other due to their referring to the same chemical compound.

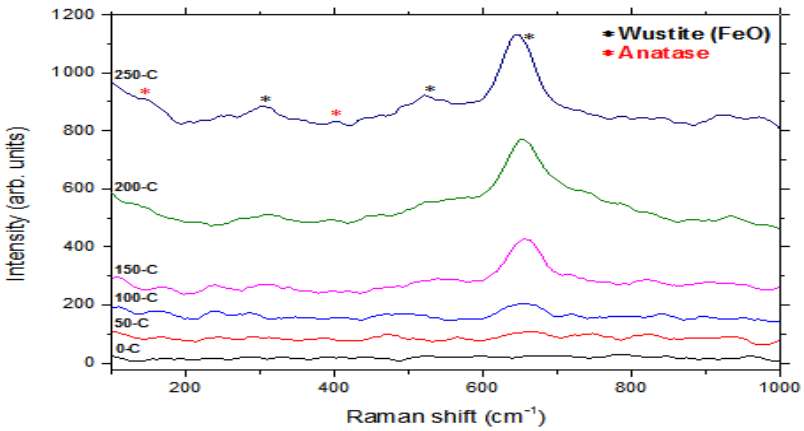

Fig. 5. Raman spectra for the samples fabricated by the ALD method from TDMAT and H_2O from 50 ALD cycles to 250 ALD cycles at a substrate temperature of 225°C. Wustite [35] and anatase [27][36] band peaks are labeled as black asterisks and red asterisks, respectively, on the spectra.

Hazanet al.[35] mentioned that the expected corrosion products for pure iron are wustite (FeO), magnetite (Fe_3O_4) and hematite (Fe_2O_3) in an oxygen-rich atmosphere; therefore, one or more of them could have been developed on the surface of our specimens because of their experimental nature. These oxide layers appear in an equal sequence to be the outer layer of an iron surface, although hematite requires temperatures above ~570°C for its presence. $Fe_{0.98}O$ formula seems to coincide with that of wustite (a range of stoichiometry for $Fe_{1-x}O$, where $0.05<x<0.16$), and their appearance is also coherent; however, wustite oxide is not thermodynamically stable at temperatures below ~570°C, and the adjacent layer to the un-oxidized surface should be magnetite. It is worth mentioning that the development of a certain iron oxide on any material and its retention can be attributed to the influence of compositional (alloying) elements, which distinctly react with oxygen; these elements could have no influence on the characteristic Raman spectrum of oxide layers.

In spite of both wustite and magnetite oxides exhibiting the same Raman peaks (the most pronounced peak is at 662 cm^{-1}, and additional medium intense peaks are at 305 cm^{-1} and 529 cm^{-1}), a difference remained in the spectra baseline below a wave-number of ~600 cm^{-1}, i.e., the spectrum baseline for wustite is more elevated than that for magnetite in this wave-number range, and it can be attributed to the FeO decomposition under illumination [35].

The aforementioned principles offer a theoretic explanation for our Raman spectra: a chemical compound ($Fe_{0.98}O$) similar to wustite has grown on the substrate surface, and it could be retained under the TiO_2 film, despite being thermodynamically unstable. In addition to the correspondence between bands for wustite spectrum cited above and bands for our spectrum, we can ensure that a compound like this has grown on the surface due to the similarity of their respective spectra baseline. There are nevertheless blue shifts for the peaks at 521 cm^{-1} and 648 cm^{-1} in comparison with those of citation that can be assigned to fine differences in chemical composition for these compounds. Microstructural changes for our substrate are further detailed by RS owing to the resolution limit of the Raman equipment, and it is exposed by allowing for the checking of the $Fe_{0.98}O$ formation from 50-C to 250-C (it is only detected by XRD in 250-C). We can overemphasize that the change in the spectra with the ALD cycles alteration is progressive, and it is not as abrupt as that in diffractograms. By comparing 0-C spectrum with other spectra, no obvious peaks are ascribed to the pristine iron surface.

A wustite-like compound could remain unchanged, that is to say, with no transformation into magnetite, on the substrate surface as a consequence of TiO_2 layer deposition since this could act to hinder in some way the transformation, and it provides some type of stability for $Fe_{0.98}O$; this hypothesis is partially confirmed by the fact of the wustite existence below other iron oxide layers [35] and our analogous experiments for the bare support, which have revealed significant differences between coated surfaces and non-coated surfaces. Because of the rising trend for the iron oxide bands, iron oxide layer, in general, should be either growing or crystallizing in the same way as ALD cycles increases, in addition to its corresponding TiO_2 layer. In this respect, we may say that the TiO_2 film (small portion) influence is not sufficient to block the $Fe_{0.98}O$ formation or the oxidation process for the iron surface, but it is sufficient to stabilize this iron oxide in these samples. Both oxidation and deposition processes should therefore be simultaneously performed in the ALD reactor chamber.

The position for the most intense peak varies gradually with a blue shift insofar as ALD cycles rise from 150-C to 250-C, the spectra where the peak is obviously defined. This phenomenon for our Raman bands can occur due to structural changes (disorders) on the support surface that were carried out during the ALD reaction and resulted in the activation of zone-edge and/or Raman-forbidden modes [27]. The band tendency might be related to a growing crystallization for the support surface, and it could be also marked by more defined or more intense peaks and the appearance of other small peaks or shoulders with that change of ALD cycles.

A shoulder at 145 cm^{-1} and a small peak at 403 cm^{-1}, however, are attributed to the anatase phase, and they are only observed in the 250-C spectrum. This occurrence indicates that a TiO_2 thin film, i.e., a small TiO_2 portion on the support, is just detected by RS for the sample that possesses the greatest proportion of TiO_2 film among the other ones due to its fabrication conditions, which is referring to the resolution limit of the Raman equipment again. We should expect a behavior for these anatase bands in spectra as that for $Fe_{0.98}O$ bands, since TiO_2 is being deposited with each ALD cycle, as the XPS results indicated, and the anatase phase should consequently be fulfilled gradually because of a temperature effect. In this way, rising peaks indicate that anatase concentration is, in general, increasing as the ALD cycles increase.

The main Raman band for anatase is approximately 143 cm^{-1}, and it corresponds to the E_g vibration mode of anatase [14][20][27][36]. In contrast, an additional smaller peak for anatase at approximately 401 cm^{-1} corresponds to the B_{1g} vibration mode of anatase [12][27][36]. The peaks we note in the 250-C spectrum can easily coincide with these bands, and the relative intensities for our peaks are similar to those for these bands as well; therefore, anatase existence is confirmed by RS on this basis, but red shifts are shown for our peaks. Red shifts could be assigned to, as we explained before, structural changes that the TiO_2 film undergoes during its

crystallization. By considering the existence of the main band, we can suggest that there is a substantial amount of anatase in 150-C, 200-C, and 250-C, and this is increasing as ALD cycles number rises; this involves an increasing trend for crystallization with an equal variation of ALD cycles as well [20][36].

Peaks in our spectra could not be ascribed to rutile phase, and it was expected because of the elaboration conditions of our specimens. Moreover, we cannot discard the growth of amorphous TiO_2 in these spectra since there is a broadband background in the Raman spectra [14], mainly for specimens elaborated in shorter periods (<200 cycles). As we mentioned above, the amorphous phase could be obtained at low numbers of ALD cycles and the film slowly transformed into anatase phase when the number of ALD cycles increase, although fine determinations could not be achieved by Raman equipment because of its resolution limit. This behavior can be an indicator of a critical thickness necessary to develop a crystalline structure [13][20][36].

The evolution of microstructure of either film or substrate can furthermore influence the surface morphology of samples which, in turn, can be analyzed by AFM. Fig. 6 depicts the representative AFM images for certain of our samples. Surfaces with high roughness are noticeably seen in these images, and their corresponding RMS roughness values are additionally listed in Table 1.

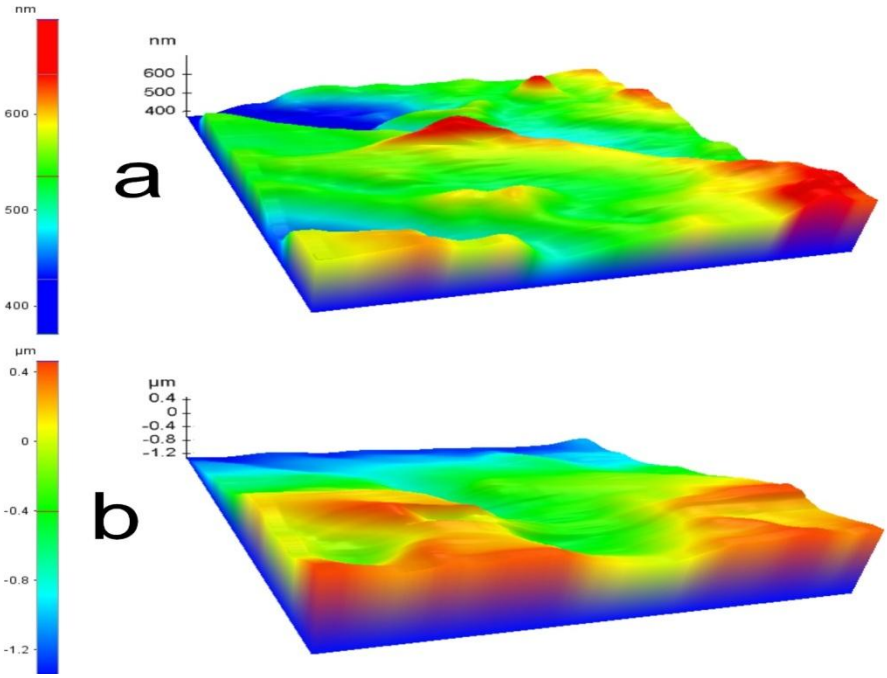

Fig. 6. AFM images for the surface topography of the selected samples 0-C (a) and 250-C (b) elaborated by the ALD method from TDMAT and H_2O at a substrate temperature of 225°C. Scanning areas represent square maps of 7.5 µm × 7.5 µm. Images rotation is x=-60, y=-25, and z=5 from their original top view.

Table 1 Calculated RMS surface roughness for the elaborated samples by the ALD method from TDMAT and H_2O at a substrate temperature of 225°C. An RMS roughness value is given by the general average of several AFM images of the same sample, and the difference between their results did not exceed the experimental uncertainty.

Sample name	RMS surface roughness(nm)
0-C	54.47
50-C	89.00
100-C	96.10
150-C	103.82
200-C	281.23
250-C	495.00

AFM images exhibit discontinuous flat areas surrounded by local dents of approximately 150 nm and various micro-blisters or bumps with an elevation fluctuating up to 350 nm. These characteristics were retained disregarding the number of ALD cycles. Oriented linear scratches were evident in these AFM maps, and they were related to the sandpapers that were used during manual polishing according to Marin's et al.[15] reports. This type of surface was expected due to manual polishing with the sandpapers we used since 180 grit and 1000 grit only lessen the substrate surface roughness up to a certain degree. A considerably longer time should be

invested in terms of preparation for our substrates in order to accomplish a low-roughness surface, although inherent costs and benefits should be also assessed.

One can note that the RMS roughness grew as the ALD cycles increased, i.e., the thicker is the film is, the higher the TiO_2 film roughness is; therefore, similar to other researchers [13][14][29], we can speculate that the film roughness will be directly dictated by the number of ALD cycles. However, there are huge alterations in the quantification of RMS roughness values from 150-C to 250-C, which eventually reach almost a fivefold RMS roughness value in comparison with that of 150-C. These alterations were therefore attributed to a temperature effect (thermal treatment-like ALD process) and the microstructural changes for film and support that we previously discussed. In our case, these phenomena seem to boost a detrimental formation for the surface roughness due to their excessively modifying the specimen surface, and this could hamper a uniform deposition of a TiO_2 film. In spite of the high-roughness surfaces we obtained, the preparation procedure for the support should not be deemed detrimental for the specimen surface since that type of surface provides more area for TiO_2 film loading, which is crucial for assembling the photocatalytic reactions [26].

Heikkiläet al.[29] reported that the RMS roughness of TiO_2 films is mostly defined by its underlying support roughness, and coatings should conform to it; hence, our RMS roughness values could be induced by the iron support. 0-C has a high RMS roughness value, that is to say, a significant rough surface, which could induce higher values because of its microstructural changes. The importance of substrate preparation upon surface roughness for samples is corroborated by comparisons, and we have not attained results that resemble those of Abendrothet al.[10] or Bratvoldet al.[16], who worked with similar ALD cycles and at the same substrate temperature, respectively. This finding was nevertheless expected due to their having utilized a smooth silicon substrate, which was entirely unlike our featureless substrate.

Surface morphology was furthermore examined by SEM, and Fig. 7 (a), (b) and(c) shows typical top-view SEM images for 0-C and 250-C, respectively, in cases of different magnifications. We can underline that there is no prominent change regarding their surface textures with the ALD cycles variations, thus confirming AFM observations and precluding a contradictory tendency for samples that have been described in the Buchalskaet al.[13] research. It must be remarked that there are no obvious morphological differences between images for 0-C and images for 250-C, although XRD and RS analyses have suggested substantial microstructural changes for the latter sample. It is also unclear whether the TiO_2 deposition is fulfilled in these images due to equipment not being able to expose as thin a film as that of the TiO_2 layer.

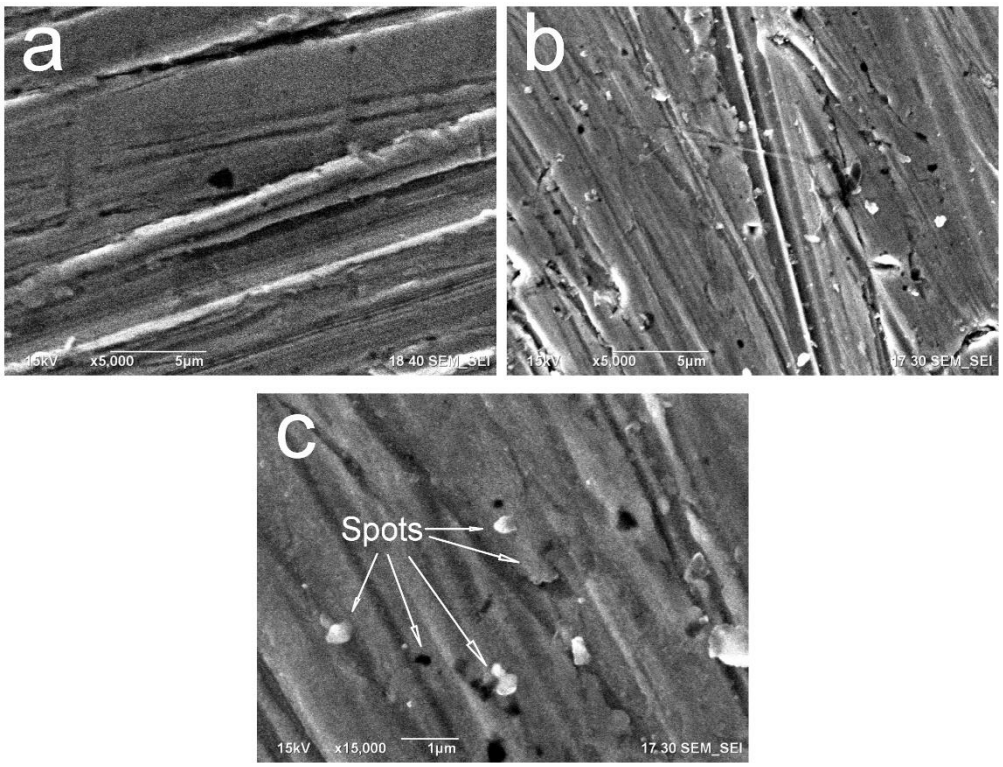

Fig. 7. SEM micrographs for the surface morphology of the elaborated samples 0-C (a) and 250-C (b) (c) by the ALD method from TDMAT and H_2O at a substrate temperature of 225°C. Images were recorded at a magnification of x5000 (a, b) or x15000 (c) at an accelerating voltage of 15 kV.

Visibly eroded surfaces are exposed from the initial micrograph/photo to the last one. Either narrow or broad arrangements of scratches that run aligned with multiple directions in the micrograph space are seen owing to the sandpapers in accordance with the aforementioned AFM results. Surface architecture is apparently deteriorated or collapsed by the manual polishing; however, we emphasize that this type of surface is beneficial for the loading of a TiO_2 film.

All of these images always exhibit terminated surfaces with isolated coarse spots with irregular shapes, and those spots are randomly distributed. This type of grain-like island appears with multiple sizes. It is assumed that these spots were developed by the preparation procedure, since this method could form irregular iron grains (particles), as well as scratches when sandpapers are polishing the surfaces.

IV. CONCLUSIONS

We have achieved depositions of crystalline TiO2 thin films on a commercial-grade iron support by the ALD process from TDMAT and de-ionized H2O as titanium and oxygen precursors, respectively. Depositions gradually took place with each ALD cycle circumventing the special support nature, and its preparation and the anatase phase was fulfilled in the same way due to a temperature effect, although a critical thickness could be necessary for it; these results open a new avenue for future studies in multiple research fields, e.g., photocatalysis.

XPS analyses conclusively exhibited that the support was being covered by titanium as ALD cycles increased and the stoichiometric composition of TiO2 formula was roughly demonstrated for our samples. Silicon impurities appeared due to the sandpapers, and they should be retained either close to the film surface or underneath it. However, the surface carbon contamination is checked regardless of ALD cycles, which is strongly governed by the naturally adsorbed atmospheric carbon contributions. No nitrogen residues were detected. XRD patterns show the development of an iron oxide because of the thermal treatment-like ALD process that oxidizes the support surface. However, no reflections ascribed to TiO2 crystalline phases were found due to the detection limit for the XRD equipment. Raman spectra exposed a more detailed formation of Fe0.98O that corresponds to a wustite-like compound, and this can be stabilized by the TiO2 layer deposition. RS studies conclude the TiO2 film crystallization, but we cannot discard the growth of amorphous TiO2. All of the AFM or SEM images exhibit rough surfaces with linear scratches owing to the sandpapers. This type of surface was expected since the substrate surface roughness is only lowered up to a certain degree by the manual polishing. A considerably longer time should be invested in terms of preparation for our substrates in order to accomplish a low-roughness surface, although inherent costs and benefits should also be assessed. The RMS roughness was induced by the substrate surface, which is affected by the thermal treatment-like effect, thus giving rise to huge increments in those values.

The results described in this study provide deep insight into the fabrication of thin TiO2 films on an iron support, and they might be considered to be a paradigm shift in the use of new substrates with simple preparation for ALD processes; they can serve as a beacon for uncertain technologies. It is worth mentioning that detailed studies concerning the catalytic properties of these samples are currently under investigation in our laboratory, where the aim is to determine their viability to act as functional photocatalysts, and this research will be published elsewhere.

REFERENCES

[1]. Z. Xie, X. Liu, W. Wang, X. Wang, C. Liu, Q. Xie, Z. Li, Z. Zhang, Enhanced photoelectrochemical and photocatalytic performance of TiO2 nanorod arrays/CdS quantum dots by coating TiO2 through atomic layer deposition, Nano Energy. 11 (2015) 400–408. doi:10.1016/j.nanoen.2014.11.024.

[2]. J. Lei, X. Li, W. Li, F. Sun, D. Lu, J. Yi, Arrayed porous iron-doped TiO2 as photoelectrocatalyst with controllable pore size, Int. J. Hydrogen Energy. 36 (2011) 8167–8172. doi:10.1016/j.ijhydene.2011.03.121.

[3]. K. Li, H. Zhang, T. Tang, Y. Xu, D. Ying, Y. Wang, J. Jia, Optimization and application of TiO2/Ti-Pt photo fuel cell (PFC) to effectively generate electricity and degrade organic pollutants simultaneously, Water Res. 62 (2014) 1–10. doi:10.1016/j.watres.2014.05.044.

[4]. S. Lu, S.-S. Sun, R. Geng, J. Gao, Effects of modified TiO2 photoanode on the photoelectrochemical properties of dye sensitized solar cells, Thin Solid Films. 589 (2015) 8–12. doi:10.1016/j.tsf.2015.04.074.

[5]. C. Das, M. Tallarida, D. Schmeißer, Linear dichroism in ALD layers of TiO2, Environ. Earth Sci. 70 (2013) 3785–3795. doi:10.1007/s12665-013-2836-7.

[6]. J.-L. Song, X. Wang, C.C. Wong, Simple Preparation of Fluorine-Doped TiO2 Photoanode for High Performance Dye Sensitized Solar Cells, Electrochim. Acta. 173 (2015) 834–838. doi:10.1016/j.electacta.2015.05.118.

[7]. A.S. Polo, M.C. Santos, R.F.B. De Souza, W.A. Alves, Pt-Ru-TiO2 photoelectrocatalysts for methanol oxidation, J. Power Sources. 196 (2011) 872–876. doi:10.1016/j.jpowsour.2010.06.076.

[8]. V. Pore, M. Heikkilä, M. Ritala, M. Leskelä, S. Areva, Atomic layer deposition of TiO2-xNx thin films for photocatalytic applications, J. Photochem. Photobiol. A Chem. 177 (2006) 68–75. doi:10.1016/j.jphotochem.2005.05.013.

[9]. N. Baram, D. Starosvetsky, J. Starosvetsky, M. Epshtein, R. Armon, Y. Ein-Eli, Enhanced inactivation of E. coli bacteria using immobilized porous TiO2 photoelectrocatalysis, Electrochim. Acta. 54 (2009) 3381–3386. doi:10.1016/j.electacta.2008.12.033.

[10]. B. Abendroth, T. Moebus, S. Rentrop, R. Strohmeyer, M. Vinnichenko, T. Weling, H. Stöcker, D.C. Meyer, Atomic layer deposition of TiO2 from tetrakis(dimethylamino) titanium and H2O, Thin Solid Films. 545 (2013) 176–182. doi:10.1016/j.tsf.2013.07.076.

[11]. A. Purniawan, G. Pandraud, T.S.Y. Moh, A. Marthen, K.A. Vakalopoulos, P.J. French, P.M. Sarro, Fabrication and optical measurements of a TiO2-ALD evanescent waveguide sensor, Sensors Actuators, A Phys. 188 (2012) 127–132. doi:10.1016/j.sna.2012.05.037.

[12]. L. Wen, B. Liu, X. Zhao, K. Nakata, A. Fujishima, Pre-treating sputtered TiO2 film by photoelectrocatalysis to increase the performance of photo-activity and photoinducedhydrophilicity, J. Electroanal. Chem. 688 (2013) 224–227. doi:10.1016/j.jelechem.2012.10.019.

[13]. M. Buchalska, M. Surówka, J. Hämäläinen, T. Iivonen, M. Leskelä, W. Macyk, Photocatalytic activity of TiO 2 films on Si support prepared by atomic layer deposition, Catal. Today. 252 (2015) 14–19. doi:10.1016/j.cattod.2014.09.032.

[14]. L. Avril, S. Reymond-Laruinaz, J.M. Decams, S. Bruy??re, V. Potin, M.C.M. De Lucas, L. Imhoff, TiO2 anatase films obtained by direct liquid injection atomic layer deposition at low temperature, Appl. Surf. Sci. 288 (2014) 201–207. doi:10.1016/j.apsusc.2013.10.007.

[15]. E. Marin, A. Lanzutti, M. Lekka, L. Guzman, W. Ensinger, L. Fedrizzi, Surface & Coatings Technology Chemical and mechanical characterization of TiO 2 / Al 2 O 3 atomic layer depositions on AISI 316 L stainless steel, Surf. Coat. Technol. 211 (2012) 84–88. doi:10.1016/j.surfcoat.2011.08.026.

[16]. J.E. Bratvold, H. Fjellvåg, O. Nilsen, Atomic Layer Deposition of oriented nickel titanate (NiTiO3), Appl. Surf. Sci. 311 (2014) 478–483. doi:10.1016/j.apsusc.2014.05.092.

[17]. L. Avril, J.M. Decams, L. Imhoff, Pulsed direct liquid injection ALD of TiO2 films using titanium tetraisopropoxide precursor, Phys. Procedia. 46 (2013) 33–39. doi:10.1016/j.phpro.2013.07.063.

[18]. Q. Xie, Y.-L. Jiang, C. Detavernier, D. Deduytsche, R.L. Van Meirhaeghe, G.-P. Ru, B.-Z. Li, X.-P. Qu, Atomic layer deposition of TiO2 from tetrakis-dimethyl-amido titanium or Ti isopropoxide precursors and H2O, J. Appl. Phys. 102 (2007) 83521. doi:10.1063/1.2798384.

[19]. K. Kanomata, P. Pansila, B. Ahmmad, S. Kubota, K. Hirahara, F. Hirose, Infrared study on room-temperature atomic layer deposition of TiO2 using tetrakis(dimethylamino)titanium and remote-plasma-excited water vapor, Appl. Surf. Sci. 308 (2014) 328–332. doi:10.1016/j.apsusc.2014.04.166.

[20]. L. Aarik, T. Arroval, R. Rammula, H. Mändar, V. Sammelselg, J. Aarik, Atomic layer deposition of TiO2 from TiCl4 and O 3, Thin Solid Films. 542 (2013) 100–107. doi:10.1016/j.tsf.2013.06.074.

[21]. Z. Zhang, X. Chang, A. Chen, Determination of chemical oxygen demand based on photoelectrocatalysis of nanoporous TiO2 electrodes, Sensors Actuators, B Chem. 223 (2016) 664–670. doi:10.1016/j.snb.2015.10.001.

[22]. E.R.A. Ferraz, G.A.R. Oliveira, M.D. Grando, T.M. Lizier, M.V.B. Zanoni, D.P. Oliveira, Photoelectrocatalysis based on Ti/TiO2 nanotubes removes toxic properties of the azo dyes Disperse Red 1, Disperse Red 13 and Disperse Orange 1 from aqueous chloride samples, J. Environ. Manage. 124 (2013) 108–114. doi:10.1016/j.jenvman.2013.03.033.

[23]. J.W. Nam, K.D. Kim, D.W. Kim, H.O. Seo, Y.D. Kim, D.C. Lim, CO oxidation of bare and TiO2-coated NiO-Ni(OH)2 nanoparticles, Curr. Appl. Phys. 12 (2012) 429–433. doi:10.1016/j.cap.2011.07.044.

[24]. K.D. Kim, D.C. Lim, H.O. Seo, J.Y. Lee, B.Y. Seo, D.J. Lee, Y. Song, S. Cho, J.H. Lim, Y.D. Kim, Enhanced performance of organic photovoltaics by TiO2-interlayer with precisely controlled thickness between ZnO electron collecting and active layers, Appl. Surf. Sci. 279 (2013) 380–383. doi:10.1016/j.apsusc.2013.04.119.

[25]. A. Ghobadi, H.I. Yavuz, T.G. Ulusoy, K.C. Icli, M. Ozenbas, A.K. Okyay, Enhanced Performance of Nanowire-Based All-TiO2 Solar Cells using Subnanometer-Thick Atomic Layer Deposited ZnO Embedded Layer, Electrochim. Acta. 157 (2015) 23–30. doi:10.1016/j.electacta.2015.01.079.

[26]. H. HU, W. jun XIAO, J. YUAN, J. wei SHI, M. xia CHEN, W. feng SHANG GUAN, Preparations of TiO2 film coated on foam nickel substrate by sol-gel processes and its photocatalytic activity for degradation of acetaldehyde, J. Environ. Sci. 19 (2007) 80–85. doi:10.1016/S1001-0742(07)60013-8.

[27]. Q. Liu, D. Ding, C. Ning, X. Wang, Black Ni-doped TiO2 photoanodes for high-efficiency photoelectrochemical water-splitting, Int. J. Hydrogen Energy. 40 (2015) 2107–2114. doi:10.1016/j.ijhydene.2014.12.064.

[28]. M.M. Momeni, Y. Ghayeb, Fabrication, characterization and photoelectrochemical performance of chromium-sensitized titania nanotubes as efficient photoanodes for solar water splitting, J. Solid State Electrochem. 20 (2016) 683–689. doi:10.1007/s10008-015-3093-3.

[29]. M. Heikkilä, E. Puukilainen, M. Ritala, M. Leskelä, Effect of thickness of ALD grown TiO2 films on photoelectrocatalysis, J. Photochem. Photobiol. A Chem. 204 (2009) 200–208. doi:10.1016/j.jphotochem.2009.03.019.

[30]. M. Zhou, X. Ma, Efficient photoelectrocatalytic activity of TiO2/Ti anode fabricated by metalorganic chemical vapor deposition (MOCVD), Electrochem. Commun. 11 (2009) 921–924. doi:10.1016/j.elecom.2009.02.029.

[31]. P.S. Shinde, P.S. Patil, P.N. Bhosale, A. Brüger, G. Nauer, M. Neumann-Spallart, C.H. Bhosale, UVA and solar light assisted photoelectrocatalytic degradation of AO7 dye in water using spray deposited TiO2 thin films, Appl. Catal. B Environ. 89 (2009) 288–294. doi:10.1016/j.apcatb.2009.02.025.

[32]. Y. Xiaoli, S. Huixiang, W. Dahui, Photoelectrocatalytic Degradation of Phenol Using a TiO 2 / Ni Thin-film Electrode, 20 (2003) 679–684.

[33]. W.Y. Gan, H. Zhao, R. Amal, Photoelectrocatalytic activity of mesoporous TiO2 thin film electrodes, Appl. Catal. A Gen. 354 (2009) 8–16. doi:10.1016/j.apcata.2008.10.054.

[34]. C. Pablos, J. Marugán, R. Van Grieken, C. Adán, A. Riquelme, J. Palma, Correlation between photoelectrochemicalbehaviour and photoelectrocatalytic activity and scaling-up of P25-TiO2 electrodes, Electrochim. Acta. 130 (2014) 261–270. doi:10.1016/j.electacta.2014.03.038.

[35]. E. Hazan, Y. Sadia, Y. Gelbstein, Characterization of AISI 4340 corrosion products using Raman spectroscopy, Corros. Sci. 74 (2013) 414–418. doi:10.1016/j.corsci.2013.05.002.

[36]. J. Shang, W. Li, Y. Zhu, Structure and photocatalytic characteristics of TiO2 film photocatalyst coated on stainless steel webnet, J. Mol. Catal. A Chem. 202 (2003) 187–195. doi:10.1016/S1381-1169(03)00200-0.

Jose Apolinar Cortes. "Atomic Layer Deposition Of TiO2 From Tetrakis (Dimethylamino) Titanium And H2O On Commercial-Grade Iron: A Simple Method For Support Preparation "International Refereed Journal of Engineering and Science (IRJES), vol. 07, no. 08, 2018, pp. 01-11